Soil Dynamics and Earthquake Engineering 29 (2009) 677–692

Contents lists available at ScienceDirect

Soil Dynamics and Earthquake Engineering

journal homepage: www.elsevier.com/locate/soildyn

Impedance matrices for circular foundation embedded in layered medium

Gin-Show Liou *, I.L. Chung

Department of Civil Engineering, Chao-Tung University, Hsin-Chu, Taiwan 30049, Taiwan

ARTICLE INFO

Article history:
Received 17 April 2008
Accepted 16 July 2008

Keywords:
Wave propagation
Impedance matrix
Dynamic stiffness
Soil–structure interaction

ABSTRACT

A numerical scheme is developed in the paper for calculating torsional, vertical, horizontal, coupling and rocking impedances in frequency domain for axial-symmetric foundations embedded in layered media. In the scheme, the whole soil domain is divided into interior and exterior domains. For the exterior domain, the analytic solutions with unknown coefficients are obtained by solving three-dimensional (3D) wave equations in cylindrical coordinates satisfying homogeneous boundary conditions. For the interior domain, the analytical solutions are also obtained by solving the same 3D wave equations satisfying the homogeneous boundary conditions and the prescribed boundary conditions. The prescribed conditions are the interaction tractions at the interfaces between embedded foundation and surrounding soil. The interaction tractions are assumed to be piecewise linear. The piecewise linear tractions at the bottom surface of foundation will be decomposed into a series of Bessel functions which can be easily fitted into the general solutions of wave equations in cylindrical coordinates. After all the analytic solutions with unknown coefficients for both interior and exterior domains are found, the variational principle is employed using the continuity conditions (both displacements and stresses) at the interfaces between interior and exterior domains, interior domain and foundation, and exterior domain and foundation to find impedance functions.

Some numerical results of torsional, vertical, horizontal, coupling and rocking impedances with different embedded depths will be presented and comments on the numerical scheme will be given.

1. Introduction

Soil–structure interaction effect plays important roles in the seismic analysis of heavy and stiff structures. Many approaches may be considered to deal with the soil–structure interaction analysis problems. Along with the substructure method, hybrid modelling of soil domain can be employed to investigate soil–structure interaction effects. In hybrid modelling, the far-field of a semi-infinite soil domain is represented by an impedance matrix at the interface of the far-field and the near-field. Finite element method is used for the near-field [1]. Also, several modelling techniques have been developed for infinite soil medium. These included viscous boundary [2,3], transmitting boundary [4], boundary element method [5], and infinite element methods [6]. Among the above mentioned modelling, boundary element method requires boundary discretization which can reduce some computational cost while compared to that of finite element method. In boundary element method, Green function is used as a fundamental solution to generate the impedance functions at the assumed boundary of structure [7]. However, using Green function in the formulation, one has to deal with the singularity problem. To avoid this situation, the analytical solutions for the layered medium with prescribed harmonic displacement time history on the surface are derived by Liou [8].

To obtain the impedance matrix for the surface foundation, some analytic approaches are available [9–12]. In these analytical approaches, the interaction tractions at the interface of foundation and soil medium are assumed to be piecewise linear or piecewise constant.

Regarding analytical or semi-analytical approaches for embedded foundation, Aviles and Perez-Rocha [13] solved the problem of torsional impedance for foundation embedded in layered medium, Tassoulas and Kansel [14] used layer elements to obtain torsional, vertical, horizontal, and rocking impedance functions, and Wolf and Preisig [15] employed cone model to calculate impedance functions.

In this paper a numerical scheme is developed to generate complete impedance functions for foundation embedded in layered medium. The impedance functions will be frequency-dependent functions. To obtain the impedances, the analytical solutions of three-dimensional (3D) wave equations in cylindrical coordinates in layered medium with satisfying the necessary boundary conditions are employed [8]. In the process of

* Corresponding author. Tel.: +886 3 5131469; fax: +886 3 5716257.
E-mail address: gsliou@mail.nctu.edu.tw (G.-S. Liou).

0267-7261/$ - see front matter © 2008 Elsevier Ltd. All rights reserved.
doi:10.1016/j.soildyn.2008.07.004

formulating the impedances, the soil medium is divided into interior and exterior domains. The analytical solutions are formed separately with unknown coefficients for both domains. And the interaction stresses at the interface between foundation and surrounding soil are assumed to be piecewise linear in z direction or r direction of the cylindrical coordinates. Then, the continuity conditions of stresses and displacements at the interface between both domains and the interface between the foundation and surrounding soil are applied to generate the impedance functions. In the process of applying the continuity conditions and generating the impedance functions, variational principle and reciprocal theorem are employed.

Some numerical aspects will be investigated in order to show the effectiveness and efficiency of the presented scheme. And the results for torsional, vertical, horizontal, coupling and rocking impedances of a cylindrical foundation embedded with different depths will also be presented to show the importance of embedment effect.

2. Derivations for 3D wave progation problems

The total soil system with prescribed tractions $t_{b1}\,e^{i\omega t}$ and $t_{b2}\,e^{i\omega t}$ having time-harmonic variations at the sidewall and the bottom of the cylindrical cavity, respectively, is shown in Fig. 1. The prescribed tractions can be expressed in terms of Fourier components with respect to the azimuth as follows:

$$t_{b1}(\theta,z)=\sum_{n=0}^{\infty}F(\theta)t_{b1}^{n}(z)$$
$$=\sum_{n=0}^{\infty}\begin{bmatrix}\sigma_{rr}^{n}(z)\begin{Bmatrix}\cos(n\theta)\\ \sin(n\theta)\end{Bmatrix}\\ \tau_{rz}^{n}(z)\begin{Bmatrix}\cos(n\theta)\\ \sin(n\theta)\end{Bmatrix}\\ \tau_{r\theta}^{n}(z)\begin{Bmatrix}-\sin(n\theta)\\ \cos(n\theta)\end{Bmatrix}\end{bmatrix}$$
$$r=a_0 \text{ and } 0\leqslant z\leqslant d \tag{1}$$

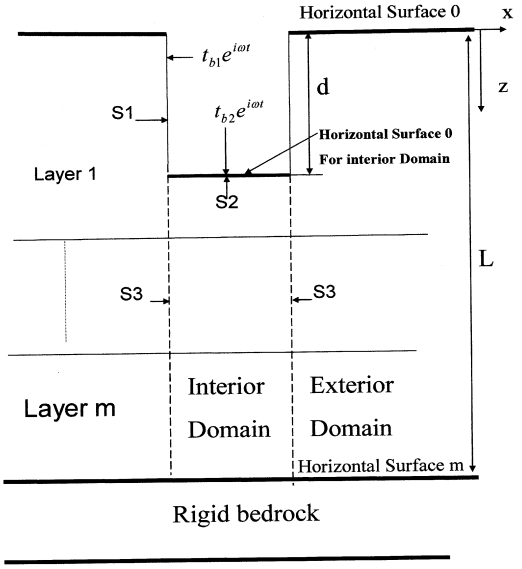

Fig. 1. Total soil system with prescribed tractions.

and

$$t_{b2}(\theta,r)=\sum_{n=0}^{\infty}F(\theta)t_{b2}^{n}(r)$$
$$=\sum_{n=0}^{\infty}\begin{bmatrix}\tau_{rz}^{n}(r)\begin{Bmatrix}\cos(n\theta)\\ \sin(n\theta)\end{Bmatrix}\\ \sigma_{zz}^{n}(r)\begin{Bmatrix}\cos(n\theta)\\ \sin(n\theta)\end{Bmatrix}\\ \tau_{\theta z}^{n}(r)\begin{Bmatrix}-\sin(n\theta)\\ \cos(n\theta)\end{Bmatrix}\end{bmatrix}$$
$$z=d \text{ and } 0\leqslant r\leqslant a_0 \tag{2}$$

where $\sigma_{rr}^{n}(z)$, $\tau_{rz}^{n}(z)$, $\tau_{r\theta}^{n}(z)$, $\tau_{rz}^{n}(r)$, $\sigma_{zz}^{n}(r)$, $\tau_{\theta z}^{n}(r)$ are the stress amplitudes of the nth Fourier component (either a symmetric component or an anti-symmetric component). To solve the wave propagation problem with the prescribed tractions of Eqs. (1) and (2) as shown in Fig. 1, Liou [8] has proposed a technique to decompose each Fourier component of the prescribed boundary condition at S_2 surface. This decomposed boundary condition can be easily fitted into the general solutions of 3D wave equations in cylindrical coordinates. By following the procedure of the technique, the solutions in interior domain consist of particular solutions which satisfy the boundary conditions of prescribed traction in Eq. (2) and rigid base $z=L$ in Fig. 1, and homogeneous solutions which satisfy the homogeneous boundaries at free surface (traction free) $z=d$ and rigid base $z=L$. The solutions for exterior domain contain only homogeneous solutions which satisfy the homogeneous boundaries at free surface $z=0$ and rigid base $z=L$. Since the solving process is the same for all the Fourier components, the superscript n in Eqs. (1) and (2) will be omitted in the following derivations of homogenous solutions and particular solutions.

The solution (e.g. traction) for interior domain in Fig. 1 is the combination of homogeneous and particular solutions as follows:

$$\boldsymbol{t}^{(i)}=\boldsymbol{t}_{\mathrm{h}}^{(i)}+\boldsymbol{t}_{\mathrm{p}}^{(i)} \tag{3}$$

The particular solution $\boldsymbol{t}_{\mathrm{p}}^{(i)}$ must satisfy the boundary conditions of Eq. (2) and rigid base condition $z=L$ (zero displacement), and the homogeneous solution $\boldsymbol{t}_{\mathrm{h}}^{(i)}$ satisfies the boundary conditions of rigid base and the free surface (zero traction).

From the general solutions of 3D wave equations, the stress and the displacement fields in a layer can be expressed in terms of the displacements and tractions on the upper boundary of the layer [8]. By employing the continuity conditions of displacements and tractions consecutively at the horizontal interface between two layers, one obtains

$$\boldsymbol{Y}_{m}^{(i)}=\bar{\boldsymbol{J}}\,\boldsymbol{a}_m\boldsymbol{a}_{m-1}\cdots\boldsymbol{a}_1\bar{\boldsymbol{J}}^{-1}\boldsymbol{Y}_{0}^{(i)}=\bar{\boldsymbol{J}}\,\boldsymbol{T}^{(i)}\bar{\boldsymbol{J}}^{-1}\boldsymbol{Y}_{0}^{(i)} \tag{4}$$

where $\boldsymbol{Y}_{m}^{(i)}=(\,u_r^{(i)}\quad u_z^{(i)}\quad \tau_{rz}^{(i)}\quad \sigma_{zz}^{(i)}\quad u_\theta^{(i)}\quad \tau_{\theta z}^{(i)}\,)_m^{\mathrm{T}}$ is the displacement-stress vector on the mth horizontal interface in Fig. 1, $\bar{\boldsymbol{J}}$ is the Bessel function matrix and the $\boldsymbol{a}_j$'s are the transfer matrices given by Eqs. (A.1)–(A.4) in the Appendix. Using Eqs. (A.2)–(A.4) for the matrices $\boldsymbol{a}_j$'s, $\boldsymbol{T}^{(i)}$ can be written as

$$\boldsymbol{T}^{(i)}=\begin{bmatrix}t_{11}^{(i)} & t_{12}^{(i)} & t_{13}^{(i)} & t_{14}^{(i)} & 0 & 0\\ t_{21}^{(i)} & t_{22}^{(i)} & t_{23}^{(i)} & t_{24}^{(i)} & 0 & 0\\ t_{31}^{(i)} & t_{32}^{(i)} & t_{33}^{(i)} & t_{34}^{(i)} & 0 & 0\\ t_{41}^{(i)} & t_{42}^{(i)} & t_{43}^{(i)} & t_{44}^{(i)} & & \\ 0 & 0 & 0 & 0 & t_{55}^{(i)} & t_{56}^{(i)}\\ 0 & 0 & 0 & 0 & t_{65}^{(i)} & t_{66}^{(i)}\end{bmatrix} \tag{5}$$

By applying the homogeneous boundary conditions of rigid base at $z = L$ and free surface at $z = d$, one obtains

$$\begin{bmatrix} 0 \\ 0 \\ 0 \end{bmatrix} = \boldsymbol{J} \begin{bmatrix} t_{11}^{(i)} & t_{12}^{(i)} & 0 \\ t_{21}^{(i)} & t_{22}^{(i)} & 0 \\ 0 & 0 & t_{55}^{(i)} \end{bmatrix} \boldsymbol{J}^{-1} \begin{bmatrix} u_r \\ u_z \\ u_\theta \end{bmatrix}_0 \tag{6}$$

where

$$\boldsymbol{J} = \begin{bmatrix} \boldsymbol{J}_n'(kr) & 0 & \frac{n}{r}\boldsymbol{J}_n(kr) \\ 0 & k\boldsymbol{J}_n(kr) & 0 \\ \frac{n}{r}\boldsymbol{J}_n(kr) & 0 & \boldsymbol{J}_n'(kr) \end{bmatrix} \tag{7}$$

Eq. (6) gives the transcendental equations

$$t_{11}^{(i)} t_{22}^{(i)} - t_{12}^{(i)} t_{21}^{(i)} = 0 \tag{8}$$

for the wave numbers representing Rayleigh modes, and

$$t_{55}^{(i)} = 0 \tag{9}$$

for the wave numbers representing Loves modes. For each wave number k, a root of Eq. (8) or (9), the tractions at depth z on the vertical interface (S_3 in Fig. 1) between the exterior and the interior domains can be expressed in terms of the displacement-stress vector on the free surface as follows:

$$\boldsymbol{t}_j^{(i)}(z) = (\boldsymbol{J}_1\boldsymbol{F}_1 + \boldsymbol{J}_2\boldsymbol{F}_2)e_j(z - h_{j-1})E_j^{-1}\boldsymbol{a}_{j-1}\cdots\boldsymbol{a}_1\bar{\boldsymbol{J}}^{-1}\boldsymbol{Y}_0^{(i)} \tag{10}$$

where $\boldsymbol{t}_j^{(i)}(z) = (\sigma_{rr}^{(i)} \quad \tau_{rz}^{(i)} \quad \tau_{\theta z}^{(i)})^{\mathrm{T}}|_{r=a_0}$ in the jth layer, and the matrices $\boldsymbol{J}_1$, $\boldsymbol{J}_2$, $\boldsymbol{F}_1 e_j(z - h_{j-1})E_j^{-1}$ and $\boldsymbol{F}_2 e_j(z - h_{j-1})E_j^{-1}$ are given by Eqs. (A.5)–(A.8) in the Appendix. Substituting the root of Eq. (8) into Eq. (4) and making use of the free surface conditions, one can easily show that $\bar{\boldsymbol{J}}^{-1}\boldsymbol{Y}_0^{(i)}$ in Eqs. (4) and (10) can be written as

$$\bar{\boldsymbol{J}}^{-1}\boldsymbol{Y}_0^{(i)} = (1 \quad \xi_i \quad 0 \quad 0 \quad 0 \quad 0)^{\mathrm{T}}\alpha_i^{(i)} \tag{11}$$

for the ith Rayleigh mode, in which $\xi_i = -t_{11}^{(i)}/t_{12}^{(i)} = -t_{21}^{(i)}/t_{22}^{(i)}$ and $\alpha_i^{(i)}$ is the unknown modal participation factor. Similarly, substituting the root of Eq. (9) into Eq. (4), one can obtain

$$\bar{\boldsymbol{J}}^{-1}\boldsymbol{Y}_0^{(i)} = (0 \quad 0 \quad 0 \quad 0 \quad 1 \quad 0)^{\mathrm{T}}\alpha_j^{(i)} \tag{12}$$

for the jth Love mode, in which $\alpha_j^{(i)}$ is the unknown modal participation factor. Because Eqs. (8) and (9) have an infinite number of roots, the displacement and stress fields in the interior domain can be approximated by a finite number of lower modes. Substituting Eqs. (11) and (12) into Eqs. (4) and (10), the displacement and stress vectors at the vertical interface (vertical surface S_3 in Fig. 1) due to homogeneous solutions can be implicitly expressed by the combination of these modes with unknown participation factors as follows:

$$\boldsymbol{u}_{\mathrm{h},S_3}^{(i)}(z) = \boldsymbol{N}_{\mathrm{h},S_3}^{(i)}(z)\boldsymbol{\alpha}^{(i)}, \quad r = a_0 \tag{13}$$

and

$$\boldsymbol{t}_{\mathrm{h},S_3}^{(i)}(z) = \boldsymbol{G}_{\mathrm{h},S_3}^{(i)}(z)\boldsymbol{\alpha}^{(i)}, \quad r = a_0 \tag{14}$$

where $\boldsymbol{N}^{(i)}(z)$ and $\boldsymbol{G}^{(i)}(z)$ are the matrices of modal displacements and stresses respectively, and $\boldsymbol{\alpha}^{(i)}$ is the vector of unknown modal participation factors. By use of Eqs. (11), (12) and (4), one can express the displacement and traction vectors at the surface S_2 of interior domain due to the homogeneous solutions in terms of the vector $\boldsymbol{\alpha}^{(i)}$ as follows:

$$\boldsymbol{u}_{\mathrm{h},S_2}^{(i)}(r) = \boldsymbol{N}_{\mathrm{h},S_2}^{(i)}(r)\boldsymbol{\alpha}^{(i)}, \quad z = d \tag{15}$$

and

$$\boldsymbol{t}_{\mathrm{h},S_2}^{(i)}(r) = 0, \quad z = d \tag{16}$$

To obtain the particular solutions for interior domain, the nth Fourier component of the prescribed traction in Eq. (2) can be expressed in a form compatible to finite element model of foundation structure. The variation of $t_{b2}^n(r)$ in Eq. (2) is assumed to be piecewise linear in r direction. Also, by the same reason, the variation of $t_{b1}^n(z)$ in Eq. (1) is assumed to be piecewise linear in z direction for generating impedance functions. For Eq. (1), the depth of embedded foundation d is divided into m_1 subintervals with equal width $b = d/m_1$. Then $t_{b1}^n(z)$ in Eq. (1) can be approximated as

$$\begin{aligned} \sigma_{rr}^n(z) &= \sum_{j=1}^{m1-1} h_j(z)q_j + h_0(z)q_0 + h_{m1}(z)q_{m1} \\ \tau_{rz}^n(z) &= \sum_{j=1}^{m1-1} h_j(z)p_j + h_0(z)p_0 + h_{m1}(z)p_{m1} \\ \tau_{r\theta}^n(z) &= \sum_{j=1}^{m1-1} h_j(z)s_j + h_0(z)s_0 + h_{m1}(z)s_{m1} \end{aligned} \tag{17}$$

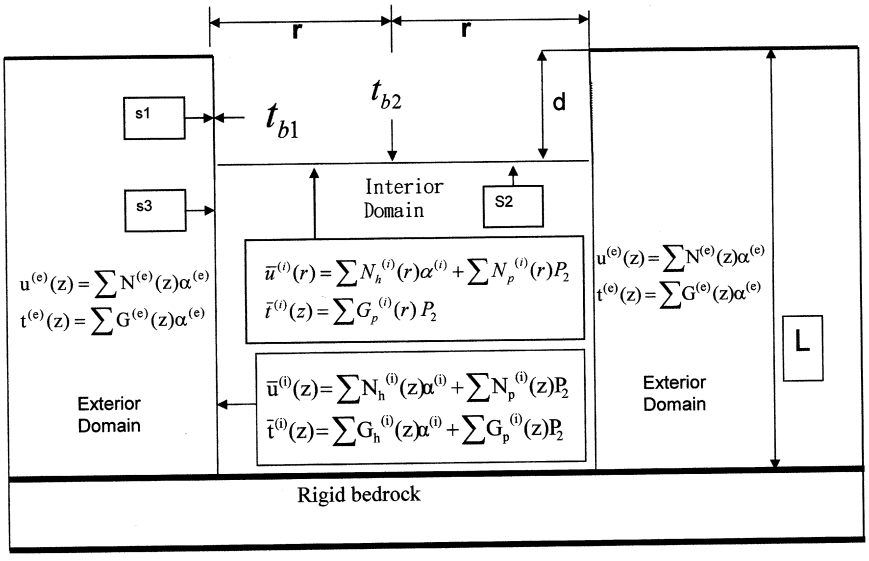

Fig. 2. Solutions at interfaces.

or

$$\boldsymbol{t}_{b1}^{n}(z) = \boldsymbol{H}_1^{\mathrm{T}}\boldsymbol{P}_1 \tag{18}$$

where

$$h_j(z) = \begin{cases} 1+\frac{z-jb}{b} & \text{if } (j-1)b \leqslant z \leqslant jb \text{ and } 1 \leqslant j \leqslant m_1 \\ 1-\frac{z-jb}{b} & \text{if } jb \leqslant z \leqslant (j+1)b \text{ and } 0 \leqslant j \leqslant m_1-1 \\ 0, & \text{otherwise,} \end{cases} \tag{19}$$

matrix $\boldsymbol{H}_1^{\mathrm{T}} = \mathrm{diag}[\boldsymbol{h}^{\mathrm{T}}, \boldsymbol{h}^{\mathrm{T}}, \boldsymbol{h}^{\mathrm{T}}]$ in which $\boldsymbol{h}^{\mathrm{T}}$ is the vector contains element $h_j(z)$ in Eqs. (19), vector $\boldsymbol{P}_1^{\mathrm{T}} = (\boldsymbol{q}^{\mathrm{T}}, \boldsymbol{p}^{\mathrm{T}}, \boldsymbol{s}^{\mathrm{T}})$ in which vectors $\boldsymbol{q}^{\mathrm{T}}$, $\boldsymbol{p}^{\mathrm{T}}$ and $\boldsymbol{s}^{\mathrm{T}}$ contains the elements q_j, p_j and s_j, respectively in Eqs. (17), and q_j, p_j and s_j are the intensities of traction at node j for $\sigma_{rr}^{n}(z)$, $\tau_{rz}^{n}(z)$ and $\tau_{r\theta}^{n}(z)$ in Eqs. (17), respectively.

Similarly, the foundation radius a_0 can be divided into m_2 subintervals and the traction $\boldsymbol{t}_{b2}^{n}(r)$ of each Fourier component in Eq. (2) can also be approximated by

$$\boldsymbol{t}_{b2}^{n}(r) = \boldsymbol{H}_2^{\mathrm{T}}\boldsymbol{P}_2 \tag{20}$$

where matrix $\boldsymbol{H}_2^{\mathrm{T}} = \mathrm{diag}[\bar{\boldsymbol{h}}^{\mathrm{T}}, \bar{\boldsymbol{h}}^{\mathrm{T}}, \bar{\boldsymbol{h}}^{\mathrm{T}}]$ with vector $\bar{\boldsymbol{h}}$ being similar to vector $\boldsymbol{h}$ defined in Eqs. (19) except the piecewise linear variable z is replaced by r, vector $\boldsymbol{P}_2^{\mathrm{T}} = (\bar{\boldsymbol{q}}^{\mathrm{T}}, \bar{\boldsymbol{p}}^{\mathrm{T}}, \bar{\boldsymbol{s}}^{\mathrm{T}})$ and $\bar{q}_j$, $\bar{p}_j$ and $\bar{s}_j$ are the intensities of traction at node j for $\tau_{rz}^{n}(r)$, $\sigma_{zz}^{n}(r)$ and $\tau_{\theta z}^{n}(r)$, respectively. It should be noted that $\boldsymbol{H}_1^{\mathrm{T}}$ and $\boldsymbol{H}_2^{\mathrm{T}}$ are $3\times 3(m_1+1)$

Table 1
Non-dimensionalized torsional impedance K_{TT}/Ga_0^3 for $d/a_0 = 0$, $L/a_0 = 2$ and $\omega a_0/\mathrm{Re}(C_s) = 0.01$

i	j	l	$m_2 = 2$	$m_2 = 3$	$m_2 = 4$	$m_2 = 5$
10	15	3	4.79+0.00059i	–	–	–
10	15	4	4.83+0.00058i	4.91+0.00061i	–	–
10	15	5	4.91+0.00056i	5.01+0.00057i	5.07+0.00055i	–
10	15	6	4.99+0.00056i	5.02+0.00053i	5.11+0.00051i	5.21+0.00048i
Liou and Lee [11]				5.254282+0.00044i		

Table 2
Non-dimensionalized vertical impedance K_{VV}/Ga_0 for $d/a_0 = 0$, $L/a_0 = 2$ and $\omega a_0/\mathrm{Re}(C_s) = 0.01$

i	j	l	$m_2 = 2$	$m_2 = 3$	$m_2 = 4$	$m_2 = 5$
10	15	3	9.27+0.0115i	–	–	–
10	15	4	9.32+0.0114i	9.38+0.0121i	–	–
10	15	5	9.33+0.0114i	9.41+0.0111i	9.43+0.0107i	–
10	15	6	9.33+0.0114i	9.43+0.0108i	9.46+0.0105i	9.62+0.0089i
Liou and Lee [11]				9.852558+0.000158i		

Table 3
Non-dimensionalized horizontal impedance K_{HH}/Ga_0^3 for $d/a_0 = 0$, $L/a_0 = 2$ and $\omega a_0/\mathrm{Re}(C_s) = 0.01$

i	j	l	$m_2 = 2$	$m_2 = 3$	$m_2 = 4$	$m_2 = 5$
10	15	3	5.746+0.0143i	–	–	–
10	15	4	5.787+0.01458i	5.846+0.0158i	–	–
10	15	5	5.783+0.01454i	5.841+0.0157i	5.921+0.00173i	–
10	15	6	5.788+0.01459i	5.855+0.0159i	5.891+0.00168i	5.966+0.0184i
Liou and Lee [11]				6.003748+0.000148 i		

Table 4
Non-dimensionalized coupling impedance K_{RH}/Ga_0^3 for $d/a_0 = 0$, $L/a_0 = 2$ and $\omega a_0/\mathrm{Re}(C_s) = 0.01$

i	j	l	$m_2 = 2$	$m_2 = 3$	$m_2 = 4$	$m_2 = 5$
10	15	3	−0.2498+0.0081i	–	–	–
10	15	4	−0.251+0.00855i	−0.219+0.0111i	–	–
10	15	5	−0.249+0.00848i	−0.227+0.0113i	−0.194+0.014i	–
10	15	6	−0.2508+0.00859i	−0.225+0.0113i	−0.204+0.0134i	−0.183+0.0167i
Liou and Lee [11]				−0.3105359−0.00003881i		

Table 5
Non-dimensionalized rocking impedance K_{RR}/Ga_0^3 for $d/a_0 = 0$, $L/a_0 = 2$ and $\omega a_0/\mathrm{Re}(C_s) = 0.01$

i	j	l	$m_2 = 2$	$m_2 = 3$	$m_2 = 4$	$m_2 = 5$
10	15	3	3.828+0.00761i	–	–	–
10	15	4	3.907+0.00761i	3.97+0.01041i	–	–
10	15	5	3.873+0.00766i	3.986+0.01033i	4.07+0.0132i	–
10	15	6	3.893+0.00758i	3.992+0.01036i	4.04+0.0129i	4.191+0.0125i
Liou and Lee [11]				4.214673+0.0003247i		

and $3\times 3(m_2{+}1)$ matrices, respectively. Because the traction $\boldsymbol{t}_{b2}^n(r)$ must be fitted in the general solutions of 3D wave equations in cylindrical coordinates for interior domain, the traction $\boldsymbol{t}_{b2}^n(r)$ can be decomposed as follows [8]:

$$\boldsymbol{t}_{b2}^n(r)=\begin{bmatrix}\tau_{rz}^n(r)\\ \sigma_{zz}^n(r)\\ \tau_{\theta z}^n(r)\end{bmatrix}=\begin{bmatrix}1\\0\\-1\end{bmatrix}\left(\frac{\tau_{rz}^n-\tau_{\theta z}^n}{2}\right)+\begin{bmatrix}0\\1\\0\end{bmatrix}(\sigma_{zz}^n)+\begin{bmatrix}1\\0\\1\end{bmatrix}\left(\frac{\tau_{rz}^n+\tau_{\theta z}^n}{2}\right) \tag{21}$$

and

$$\begin{aligned}\frac{\tau_{rz}^n(r)-\tau_{\theta z}^n(r)}{2}&=\sum_{i=1}^{\infty}k_i^{(1)}J_{n+1}(k_i^{(1)}r)A_i+k_0^{(1)}J_{n+1}(k_0^{(1)}r)A_0\\ \sigma_{zz}^n(r)&=\sum_{j=1}^{\infty}k_j^{(2)}J_n(k_j^{(2)}r)B_j+k_0^{(2)}J_n(k_0^{(2)}r)B_0\\ \frac{\tau_{rz}^n(r)+\tau_{\theta z}^n(r)}{2}&=\sum_{i=1}^{\infty}k_l^{(3)}J_{n-1}(k_l^{(3)}r)C_l+k_0^{(3)}J_{n-1}(k_0^{(3)}r)C_0\end{aligned} \tag{22}$$

where the $k_i^{(1)}$'s, $k_j^{(2)}$'s and $k_l^{(3)}$'s are the roots of $J_{n+1}(k_i^{(1)}a_0)=0$, $J_n(k_j^{(2)}a_0)=0$ and $J_{n-1}(k_l^{(3)}a_0)=0$, respectively, for i, j, $l=1,2,\ldots,\infty$, and choosing $k_0^{(1)}=0.5k_1^{(1)}$, $k_0^{(2)}=0.5k_1^{(2)}$ and $k_0^{(3)}=0.5k_1^{(3)}$ in order to satisfy the boundary condition at $r=a_0$ and $z=d$. The Bessel functions in Eqs. (22), except the first term, are orthogonal to each other with respect to the weighting function $w(r)=r$ in the interval $(0, a_0)$. The A_i's, B_j's and C_l's can be determined from the orthogonal property as follows:

$$A_0=\frac{\tau_{rz}^n(a_0)-\tau_{\theta z}^n(a_0)}{2k_0^{(1)}J_{n+1}(k_0^{(1)}a_0)} \tag{23}$$

$$A_i=\frac{\int_0^{a_0}r\left(\frac{\tau_{rz}^n-\tau_{\theta z}^n}{2}\right)J_{n+1}(k_i^{(1)}r)\,\mathrm{d}r-k_0^{(1)}A_0\int_0^{a_0}J_{n+1}(k_0^{(1)}r)J_{n+1}(k_i^{(1)}r)r\,\mathrm{d}r}{k_i^{(1)}\int_0^{a_0}J_{n+1}^2(k_i^{(1)}r)r\,\mathrm{d}r} \tag{24}$$

$$B_0=\frac{\sigma_{zz}^n(a_0)}{k_0^{(2)}J_n(k_0^{(2)}a_0)} \tag{25}$$

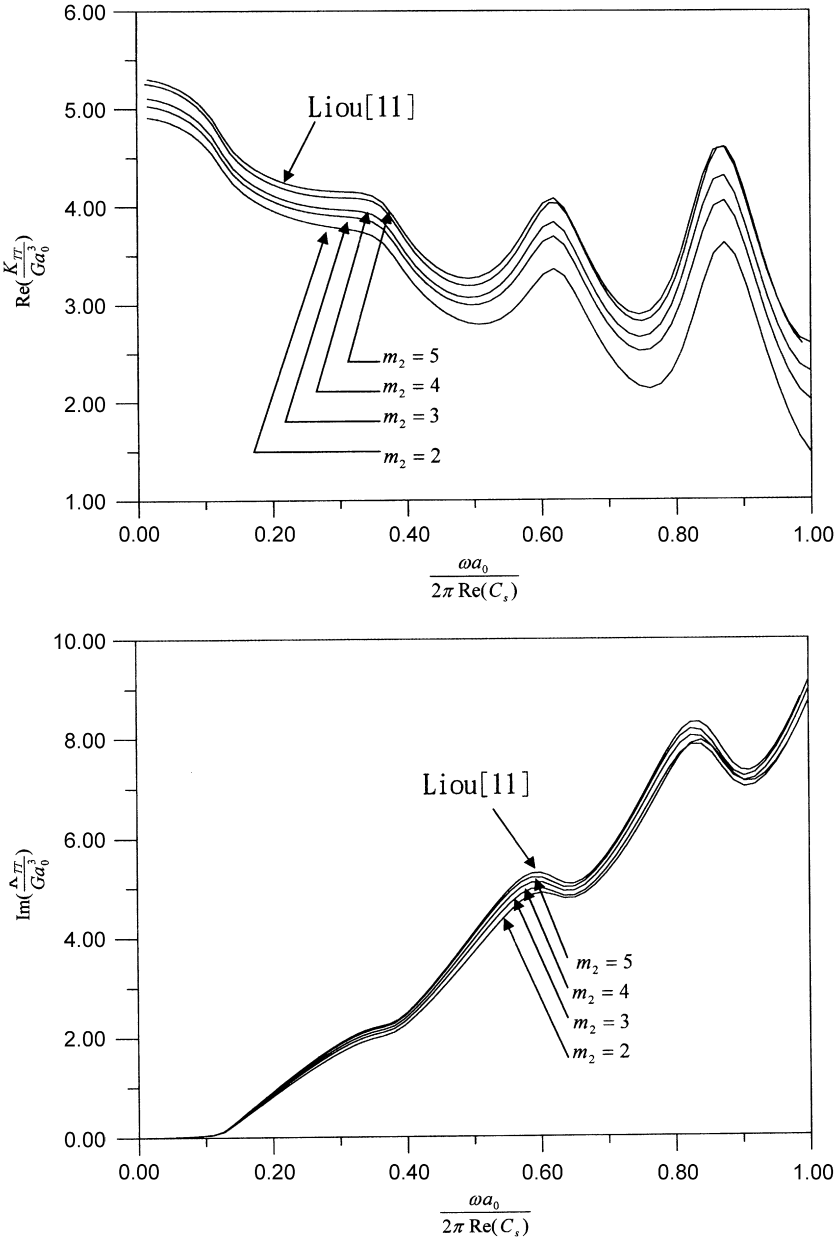

Fig. 3. Comparison of non-dimensionalized torsional impedence with Liou's results for $L/a_0=2$.

$$B_j = \frac{\int_0^{a_0} r(\sigma_{zz}^n) J_n(k_j^{(2)} r)\,\mathrm{d}r - k_0^{(2)} B_0 \int_0^{a_0} J_n(k_0^{(2)} r) J_n(k_j^{(2)} r) r\,\mathrm{d}r}{k_j^{(2)} \int_0^{a_0} J_n^2(k_j^{(2)} r) r\,\mathrm{d}r} \tag{26}$$

$$C_0 = \frac{\tau_{rz}^n(a_0) + \tau_{\theta z}^n(a_0)}{2k_0^{(3)} J_{n-1}(k_0^{(3)} a_0)} \tag{27}$$

$$C_l = \frac{\int_0^{a_0} r\left(\frac{\tau_{rz}^n + \tau_{\theta z}^n}{2}\right) J_{n-1}(k_l^{(3)} r)\,\mathrm{d}r - k_0^{(3)} C_0 \int_0^{a_0} J_{n-1}(k_0^{(3)} r) J_{n-1}(k_l^{(3)} r) r\,\mathrm{d}r}{k_l^{(3)} \int_0^{a_0} J_{n-1}^2(k_l^{(3)} r) r\,\mathrm{d}r} \tag{28}$$

In Eqs. (22), the A_i's, B_j's and C_l's are defined as the modal participation factors with respect to the wave numbers $k_i^{(1)}$'s, $k_j^{(2)}$'s and $k_l^{(3)}$'s, respectively. Since vectors $[1, \ 0, \ -1]^{\mathrm{T}}$, $[0, \ 1, \ 0]^{\mathrm{T}}$, $[1, \ 0, \ 1]^{\mathrm{T}}$ are the eigenvectors of $\boldsymbol{J}$ in Eq. (7) with respective eigenvalues $k_i J_{n+1}(k_i r)$, $k_j J_n(k_j r)$, and $k_l J_{n-1}(k_l r)$, one can substitute Eq. (20) into Eq. (21) and make use of Eqs. (22)–(28) to obtain

$$\begin{aligned}
\boldsymbol{t}_{b2}^n(r) &= \begin{bmatrix} \tau_{rz}^n(r) \\ \sigma_{zz}^n(r) \\ \tau_{\theta z}^n(r) \end{bmatrix} = \begin{bmatrix} 1 \\ 0 \\ -1 \end{bmatrix} \left(\frac{\tau_{rz}^n - \tau_{\theta z}^n}{2}\right) + \begin{bmatrix} 0 \\ 1 \\ 0 \end{bmatrix} (\sigma_{zz}^n) \\
&\quad + \begin{bmatrix} 1 \\ 0 \\ 1 \end{bmatrix} \left(\frac{\tau_{rz}^n + \tau_{\theta z}^n}{2}\right) = \left(\sum_{i=0}^{\infty} \boldsymbol{J}_n^{(1)} \begin{bmatrix} \boldsymbol{D}_i^{n+1} & 0 & -\boldsymbol{D}_i^{n+1} \\ 0 & 0 & 0 \\ -\boldsymbol{D}_i^{n+1} & 0 & \boldsymbol{D}_i^{n+1} \end{bmatrix} \right. \\
&\quad \left. + \sum_{j=0}^{\infty} \boldsymbol{J}_n^{(2)} \begin{bmatrix} 0 & 0 & 0 \\ 0 & \boldsymbol{D}_j^n & 0 \\ 0 & 0 & 0 \end{bmatrix} + \sum_{l=0}^{\infty} \boldsymbol{J}_n^{(3)} \begin{bmatrix} \boldsymbol{D}_l^{n-1} & 0 & \boldsymbol{D}_l^{n-1} \\ 0 & 0 & 0 \\ \boldsymbol{D}_l^{n-1} & 0 & \boldsymbol{D}_l^{n-1} \end{bmatrix} \right) \boldsymbol{P}_2 \\
&= \left(\sum_{i=0}^{\infty} \boldsymbol{J}_n^{(1)} \bar{\boldsymbol{D}}_i^{n+1} + \sum_{j=0}^{\infty} \boldsymbol{J}_n^{(2)} \bar{\boldsymbol{D}}_j^{n} + \sum_{l=0}^{\infty} \boldsymbol{J}_n^{(3)} \bar{\boldsymbol{D}}_l^{n-1} \right) \boldsymbol{P}_2 \\
&= \boldsymbol{G}_{\mathrm{p},S_2}^{(i)}(r) \boldsymbol{P}_2
\end{aligned} \tag{29}$$

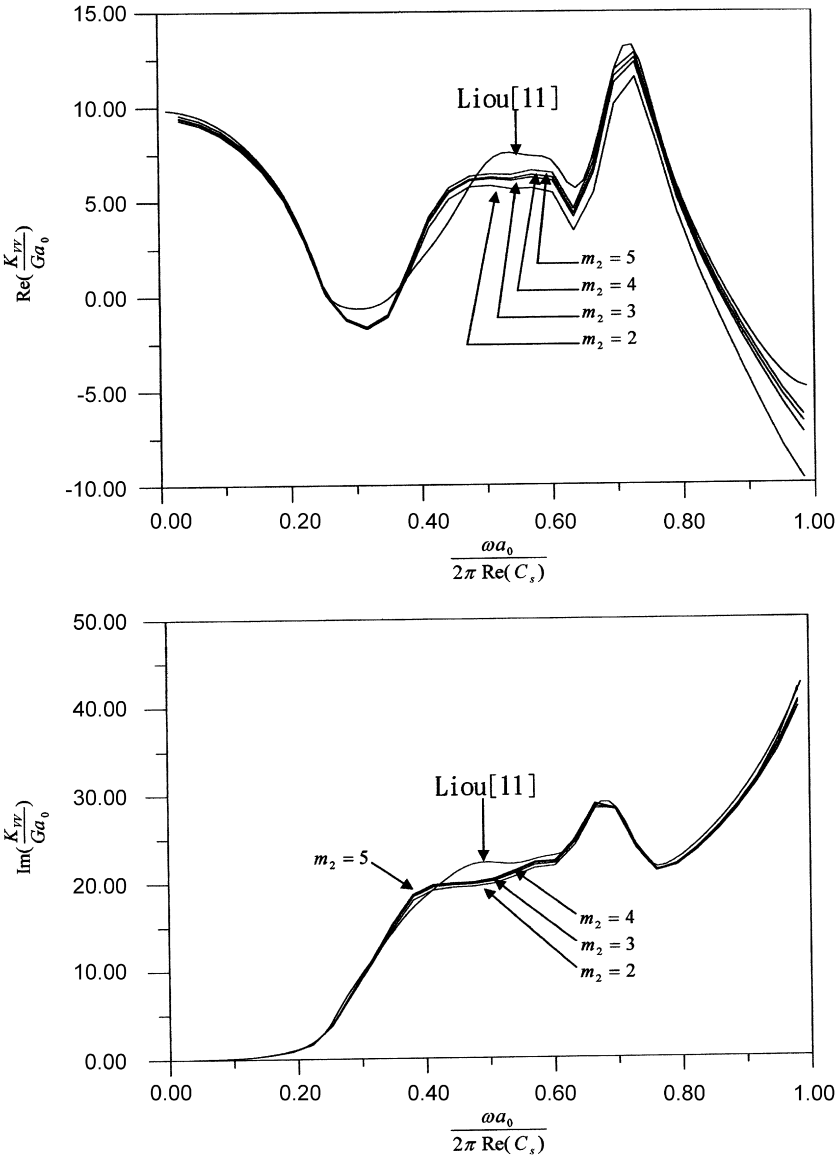

Fig. 4. Comparison of non-dimensionalized vertical impedence with Liou's results for $L/a_0 = 2$.

where

$$\boldsymbol{D}_i^{n+1} = \frac{1}{2}\int_0^{a_0} \bar{\boldsymbol{h}} J_{n+1}(k_i^{(1)} r) r \,\mathrm{d}r + \frac{1}{2}[1]\int_0^{a_0} \frac{J_{n+1}(k_0^{(1)} r) J_{n+1}(k_i^{(1)} r) r \,\mathrm{d}r}{k_0^{(1)} J_{n+1}^2(k_0^{(1)} r)} \tag{30}$$

$$\boldsymbol{D}_j^{n} = \frac{1}{2}\int_0^{a_0} \bar{\boldsymbol{h}} J_{n}(k_j^{(2)} r) r \,\mathrm{d}r + \frac{1}{2}[1]\int_0^{a_0} \frac{J_{n}(k_0^{(2)} r) J_{n}(k_j^{(2)} r) r \,\mathrm{d}r}{k_0^{(2)} J_{n}^2(k_0^{(2)} r)} \tag{31}$$

$$\boldsymbol{D}_l^{n-1} = \frac{1}{2}\int_0^{a_0} \bar{\boldsymbol{h}} J_{n-1}(k_l^{(3)} r) r \,\mathrm{d}r + \frac{1}{2}[1]\int_0^{a_0} \frac{J_{n-1}(k_0^{(3)} r) J_{n-1}(k_l^{(3)} r) r \,\mathrm{d}r}{k_0^{(3)} J_{n-1}^2(k_0^{(3)} r)} \tag{32}$$

where vector $\bar{\boldsymbol{h}}$ is defined in Eq. (20), all the elements in vector [1], except the last element is equal to 1, are 0, and $\boldsymbol{J}_n^{(1)}$, $\boldsymbol{J}_n^{(2)}$ and $\boldsymbol{J}_n^{(3)}$ are the matrix $\boldsymbol{J}$ in Eq. (7) with wave numbers $k_i^{(1)}$, $k_j^{(2)}$ and $k_l^{(3)}$, respectively. Substituting each mode in Eq. (29) into the general solutions of Eq. (4) and making use of rigid base condition $z = L$, one can obtain the displacement field at the surface S_2 of interior domain due to particular solutions as follows:

$$\boldsymbol{u}_{\mathrm{p},S_2}^{(i)}(r) = \left(\sum_{i=0}^{\infty} \boldsymbol{J}_n^{(1)} \boldsymbol{Q}_n^{(1)} \bar{\boldsymbol{D}}_i^{n+1} + \sum_{j=0}^{\infty} \boldsymbol{J}_n^{(2)} \boldsymbol{Q}_n^{(2)} \bar{\boldsymbol{D}}_j^{n} + \sum_{l=0}^{\infty} \boldsymbol{J}_n^{(3)} \boldsymbol{Q}_n^{(3)} \bar{\boldsymbol{D}}_l^{n-1}\right) \boldsymbol{P}_2 = \boldsymbol{N}_{\mathrm{p},S_2}^{(i)}(r) \boldsymbol{P}_2 \tag{33}$$

where $\boldsymbol{Q}_n^{(1)}$, $\boldsymbol{Q}_n^{(2)}$ and $\boldsymbol{Q}_n^{(3)}$ can be obtained using Eqs. (4) and (5) with wave numbers $k_i^{(1)}$, $k_j^{(2)}$, and $k_l^{(3)}$, respectively as follows:

$$\boldsymbol{Q}_n = -\begin{bmatrix} t_{11}^{(i)} & t_{12}^{(i)} & 0 \\ t_{21}^{(i)} & t_{22}^{(i)} & 0 \\ 0 & 0 & t_{55}^{(i)} \end{bmatrix}^{-1} \begin{bmatrix} t_{13}^{(i)} & t_{14}^{(i)} & 0 \\ t_{23}^{(i)} & t_{24}^{(i)} & 0 \\ 0 & 0 & t_{56}^{(i)} \end{bmatrix} \tag{34}$$

and elements $t_{ij}^{(i)}$ in Eq. (34) are defined in Eq. (5). From the derivations above, $\boldsymbol{t}_{\mathrm{p},S_2}^{(i)}(r)$ is equal to $\boldsymbol{t}_{b2}^{n}$ in Eqs. (20) or (29). For each mode in Eqs. (33) and (29), vectors $\boldsymbol{J}^{-1}\boldsymbol{u}_{\mathrm{p},S_2}^{(i)}$ and $\boldsymbol{J}^{-1}\boldsymbol{t}_{\mathrm{p},S_2}^{(i)}$ can be combined into the vectors $\bar{\boldsymbol{J}}_n^{-1}\boldsymbol{Y}_0^{(i)}$ in Eq. (10). Therefore, if one truncates high modes in Eqs. (33) and (29), the displacement and traction fields due to the prescribed traction $\boldsymbol{t}_{b2}^{n}(r)$ in Eq. (20) at

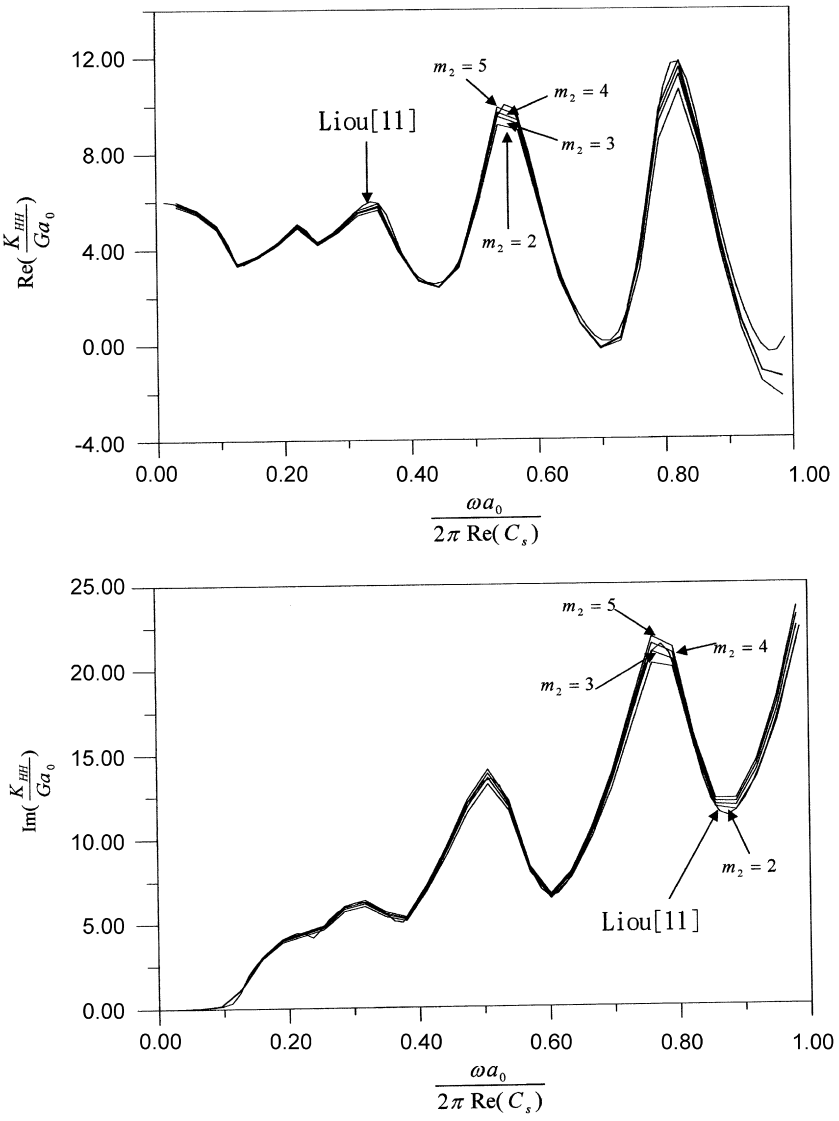

Fig. 5. Comparison of non-dimensionalized horizontal impedence with Liou's results for $L/a_0 = 2$.

the vertical interface S_3 between interior domain and exterior domains can have similar expressions to Eqs. (13) and (14), respectively.

$$\boldsymbol{u}^{(i)}_{\mathrm{p},S_3}(z) = \boldsymbol{N}^{(i)}_{\mathrm{p},S_3}(z)\boldsymbol{P}_2, \quad r = a_0 \tag{35}$$

and

$$\boldsymbol{t}^{(i)}_{\mathrm{p},S_3}(z) = \boldsymbol{G}^{(i)}_{\mathrm{p},S_3}(z)\boldsymbol{P}_2, \quad r = a_0 \tag{36}$$

For the exterior domain in Fig. 1, only homogeneous solutions are involved since the solutions have to satisfy the homogenous boundaries at $z = 0$ and L. Therefore, one just follows the procedures of finding homogeneous solutions for interior domain to obtain the solutions. To do this, one can express the displacement and stress fields in terms of displacement-stress vector at the top surface ($z = 0$) of the layered medium like the procedure to obtain Eqs. (4) and (10) except the Bessel function matrix $\bar{\boldsymbol{J}}$ is replaced with Hankel function matrix $\bar{\boldsymbol{H}}$. Matrix $\bar{\boldsymbol{H}}$ is similar to matrix $\bar{\boldsymbol{J}}$ in Eq. (A.1) except the element $J_n(kr)$ and $J'_n(kr)$ are replaced by the second kind of Hankel functions $H_n(kr)$ and $H'_n(kr)$. Then the displacement and stress at the vertical surface S_1+S_3 in Fig. 1 can be written by the combination of a finite number of modes with unknown participation factors similar to Eqs. (13) and (14).

$$\boldsymbol{u}^{(e)}_{\mathrm{h},S_1+S_3}(z) = \boldsymbol{N}^{(e)}(z)\boldsymbol{\alpha}^{(e)}, \quad r = a_0 \tag{37}$$

and

$$\boldsymbol{t}^{(e)}_{\mathrm{h},S_1+S_3}(z) = \boldsymbol{G}^{(e)}(z)\boldsymbol{\alpha}^{(e)}, \quad r = a_0 \tag{38}$$

where matrices $\boldsymbol{N}^{(e)}(z)$ and $\boldsymbol{G}^{(e)}(z)$ contain all the considered modal shapes of displacement and stress respectively, and $\boldsymbol{\alpha}^{(e)}$ is the vector of unknown modal participation factors.

3. Formulation of impedance matrix

In Fig. 2, the solutions at the boundaries of interior domain and exterior domain have been shown by using Eqs. (37) and (38) for exterior domain and Eqs. (3), (13)–(16), (20 or 29), (33), (35) and (36) for interior domain. Also, in the following derivations, the variation with respect to θ ($\cos(n\theta)$ or $\sin(n\theta)$) will be omitted in the expression, and the integrations with respect to θ will be automatically calculated. By applying the stress continuity

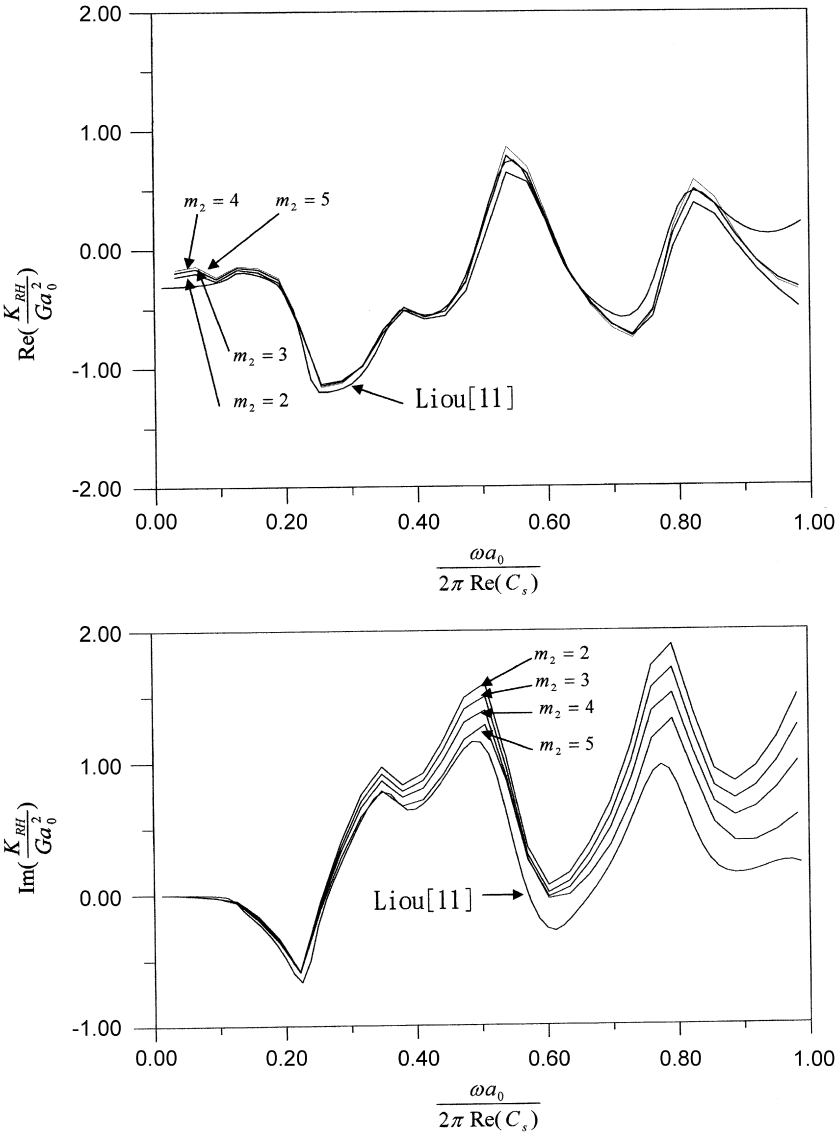

Fig. 6. Comparison of non-dimensionalized coupling impedence with Liou's results for $L/a_0 = 2$.

condition to vertical surface S_1+S_3, the variational principle $\int_{S_1+S_3} \delta \boldsymbol{u}^{(e)}(z)(\boldsymbol{t}^{(e)}(z) - \boldsymbol{t}^{(i)})\,\mathrm{d}\boldsymbol{S} = 0$ gives

$$\boldsymbol{K}_{ee}\boldsymbol{\alpha}^{(e)} - \boldsymbol{K}_{eh}\boldsymbol{\alpha}^{(i)} = \boldsymbol{K}_{ep}\boldsymbol{P}_2 - \boldsymbol{V}_{b1}\boldsymbol{P}_1 \tag{39}$$

where

$$\boldsymbol{K}_{ee} = \int_{S_1+S_3} \boldsymbol{N}^{(e)^{\mathrm{T}}}(z)\boldsymbol{G}_{\mathrm{h}}^{(e)}(z)\,\mathrm{d}\boldsymbol{S} \tag{40}$$

$$\boldsymbol{K}_{eh} = \int_{S_3} \boldsymbol{N}^{(e)^{\mathrm{T}}}(z)\boldsymbol{G}_{\mathrm{h},S_3}^{(i)}(z)\,\mathrm{d}\boldsymbol{S} \tag{41}$$

$$\boldsymbol{K}_{ep} = \int_{S_3} \boldsymbol{N}^{(e)^{\mathrm{T}}}(z)\boldsymbol{G}_{\mathrm{p},S_3}^{(i)}(z)\,\mathrm{d}\boldsymbol{S} \tag{42}$$

$$\boldsymbol{V}_{b1} = \int_{S_3} \boldsymbol{N}^{(e)^{\mathrm{T}}}(z)\boldsymbol{H}_1(z)\,\mathrm{d}\boldsymbol{S} \tag{43}$$

Similarly, imposing the displacement continuity condition, the variational principle of $\int_{S3} \delta \boldsymbol{t}^{(i)}(z)(\boldsymbol{u}^{(i)}(z) - \boldsymbol{u}^{(e)})\,\mathrm{d}\boldsymbol{S} = 0$ gives

$$-\boldsymbol{K}_{\mathrm{he}}\boldsymbol{\alpha}^{(e)} + \boldsymbol{K}_{\mathrm{hh}}\boldsymbol{\alpha}^{(i)} = -\boldsymbol{K}_{\mathrm{hp}}\boldsymbol{P}_2 \tag{44}$$

where

$$\boldsymbol{K}_{\mathrm{he}} = \int_{S_3} \boldsymbol{G}_{\mathrm{h},S_3}^{(i)^{\mathrm{T}}}(z)\boldsymbol{N}^{(e)}(z)\,\mathrm{d}\boldsymbol{S} \tag{45}$$

$$\boldsymbol{K}_{\mathrm{hh}} = \int_{S_3} \boldsymbol{G}_{\mathrm{h},S_3}^{(i)^{\mathrm{T}}}(z)\boldsymbol{N}_{\mathrm{h},S_3}^{(i)}(z)\,\mathrm{d}\boldsymbol{S} \tag{46}$$

$$\boldsymbol{K}_{\mathrm{hp}} = \int_{S_3} \boldsymbol{G}_{\mathrm{h},S_3}^{(i)^{\mathrm{T}}}(z)\boldsymbol{N}_{\mathrm{p},S_3}^{(i)}(z)\,\mathrm{d}\boldsymbol{S} \tag{47}$$

Eqs. (39) and (44) can be combined as

$$\begin{bmatrix} K_{ee} & -K_{eh} \\ -K_{he} & K_{hh} \end{bmatrix} \begin{bmatrix} \alpha_{(e)} \\ \alpha^{(i)} \end{bmatrix} = \begin{bmatrix} K_{ep} \\ -K_{hp} \end{bmatrix} \boldsymbol{P}_2 + \begin{bmatrix} -V_{b1} \\ 0 \end{bmatrix} \boldsymbol{P}_1 \tag{48}$$

Therefore, the unknown modal participation factors of the homogeneous solutions in the exterior and interior domains can be expressed in terms of the stress intensity vectors $\boldsymbol{P}_1$ and $\boldsymbol{P}_2$ in Eqs. (18) and (20), respectively, as follows:

$$\begin{bmatrix} \boldsymbol{\alpha}^{(e)} \\ \boldsymbol{\alpha}^{(i)} \end{bmatrix} = \begin{bmatrix} \xi_1 \\ \xi_2 \end{bmatrix} \boldsymbol{P}_2 + \begin{bmatrix} \xi_3 \\ \xi_4 \end{bmatrix} \boldsymbol{P}_1 \tag{49}$$

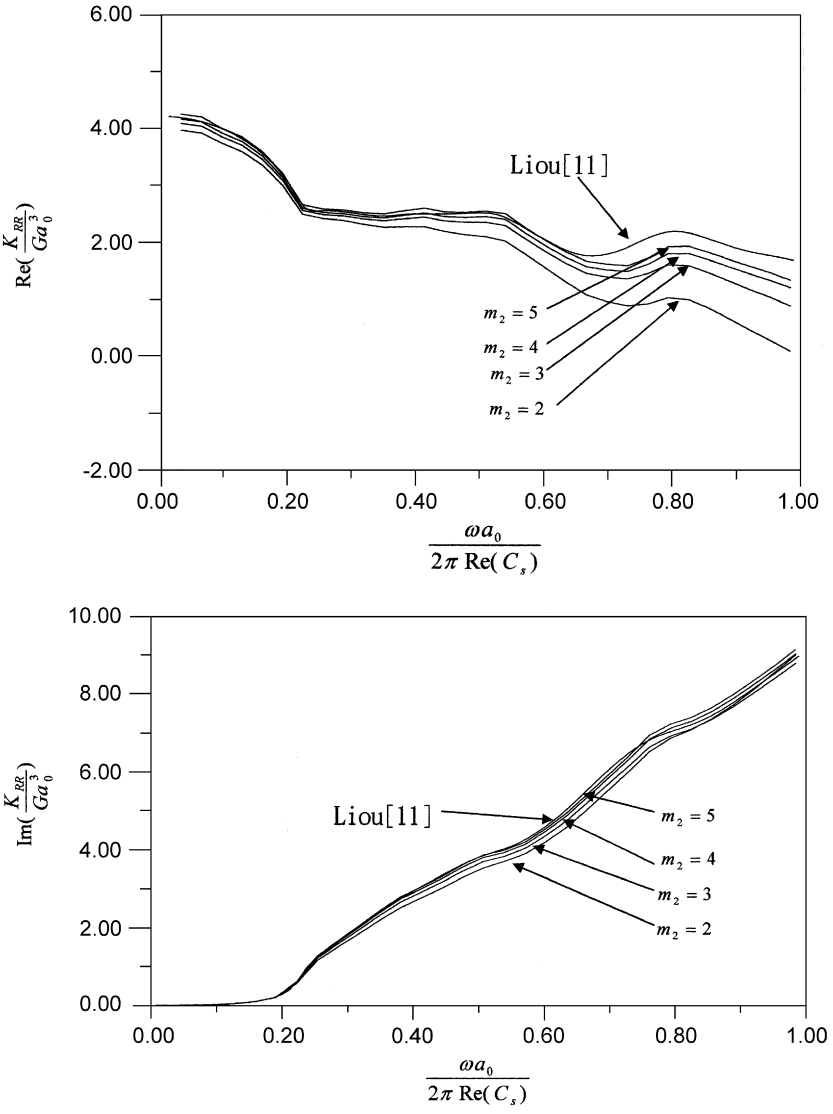

Fig. 7. Comparison of non-dimensionalized rocking impedence with Liou's results for $L/a_0 = 2$.

Consequently all the displacement and the stress components at any arbitrary location in the soil domain can be obtained for the arbitrarily prescribed piecewise linear tractions at the surface of cylindrical cavity. Now, referring to Fig. 2 and making use of Eqs. (49), (18) and (20), the displacement and traction at surfaces S_1 and S_2 can be written as

$$\boldsymbol{u}_0 = \begin{bmatrix} \boldsymbol{u}_{S_1}(z) \\ \boldsymbol{u}_{S_2}(r) \end{bmatrix} = \begin{bmatrix} \boldsymbol{N}^{(e)}(z)\xi_3 & \boldsymbol{N}^{(e)}(z)\xi_1 \\ \boldsymbol{N}^{(i)}_{\mathrm{h},S_2}(r)\xi_4 & \boldsymbol{N}^{(i)}_{\mathrm{h},S_2}(r)\xi_2 + \boldsymbol{N}^{(i)}_{\mathrm{p},S_2}(r) \end{bmatrix} \begin{bmatrix} \boldsymbol{P}_1 \\ \boldsymbol{P}_2 \end{bmatrix} \tag{50}$$

and

$$\boldsymbol{t}_0 = \begin{bmatrix} \boldsymbol{t}_{S_1}(z) \\ \boldsymbol{t}_{S_2}(r) \end{bmatrix} = \begin{bmatrix} \boldsymbol{H}_1(z) & 0 \\ 0 & \boldsymbol{H}_2(r) \end{bmatrix} \begin{bmatrix} \boldsymbol{P}_1 \\ \boldsymbol{P}_2 \end{bmatrix} \tag{51}$$

To form the impedance matrix, one can use Eqs. (50) and (51). The variational principle gives the virtual work of the system as follows:

$$\begin{aligned} \delta \boldsymbol{W} &= \int_{S1+S2} \delta \boldsymbol{t}_0^{\mathrm{T}} \boldsymbol{u}_0 \, \mathrm{d}\boldsymbol{S} = \delta \boldsymbol{P}^{\mathrm{T}} \int_{S1+S2} \begin{bmatrix} \boldsymbol{H}_1^{\mathrm{T}}(z) & 0 \\ 0 & \boldsymbol{H}_2^{\mathrm{T}}(r) \end{bmatrix} \\ &\quad \times \begin{bmatrix} \boldsymbol{N}^{(e)}(z)\xi_3 & \boldsymbol{N}^{(e)}(z)\xi_1 \\ \boldsymbol{N}^{(i)}_{\mathrm{h},S_2}(r)\xi_4 & (\boldsymbol{N}^{(i)}_{\mathrm{h},S_2}(r)\xi_2 + \boldsymbol{N}^{(i)}_{p,S_2}(r)) \end{bmatrix} \mathrm{d}\boldsymbol{S}\, \boldsymbol{P} \\ &= \delta \boldsymbol{P}^{\mathrm{T}} \begin{bmatrix} \boldsymbol{Q}_{11} & \boldsymbol{Q}_{12} \\ \boldsymbol{Q}_{21} & \boldsymbol{Q}_{22} \end{bmatrix} \boldsymbol{P} = \delta \boldsymbol{P}^{\mathrm{T}} \boldsymbol{Q} \boldsymbol{P} \end{aligned} \tag{52}$$

where

$$\boldsymbol{Q}_{11} = \int_0^d \boldsymbol{H}_1^{\mathrm{T}}(z) \boldsymbol{N}^{(e)}(z) \, \mathrm{d}z \, \xi_3 \tag{53}$$

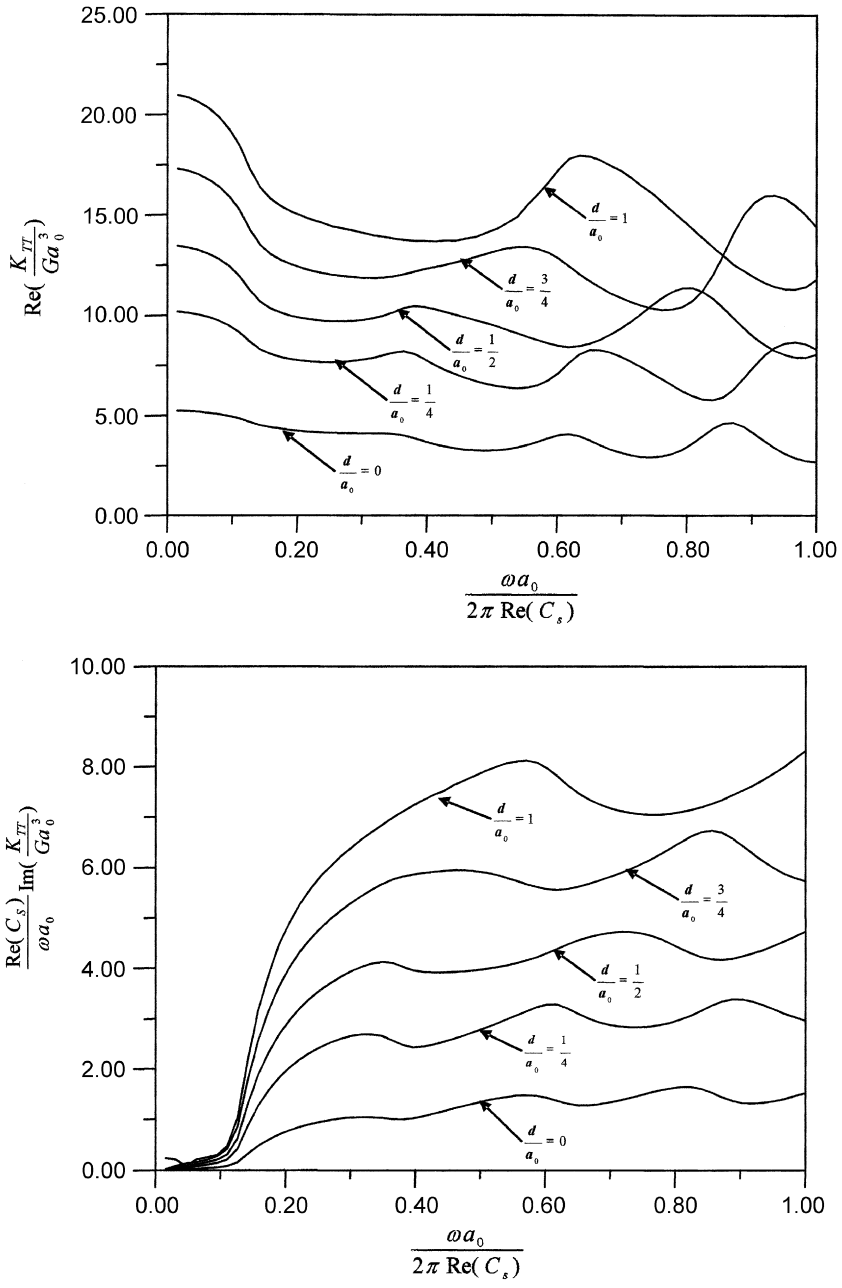

Fig. 8. Non-dimensionalized tortional impedence with different depths for $L/a_0 = 2$.

$$\boldsymbol{Q}_{12} = \int_0^d \boldsymbol{H}_1^{\mathrm{T}}(z)\boldsymbol{N}^{(e)}(z)\,\mathrm{d}z\,\xi_1 \tag{54}$$

$$\boldsymbol{Q}_{21} = \int_0^{a_0} \boldsymbol{H}_2^{\mathrm{T}}(r)\boldsymbol{N}_{\mathrm{h},S_2}^{(i)}(r) r\,\mathrm{d}r\,\xi_4 \tag{55}$$

and

$$\boldsymbol{Q}_{22} = \int_0^{a_0} \boldsymbol{H}_2^{\mathrm{T}}(r)[\boldsymbol{N}_{\mathrm{h},S_2}^{(i)}(r)\xi_2 + \boldsymbol{N}_{\mathrm{p},S_2}^{(i)}(r)] r\,\mathrm{d}r \tag{56}$$

For the foundation itself, the displacement field of the foundation for the nth Fourier component (either a symmetric or an anti-symmetric component as shown in Eqs. (1) or (2)) can be assumed as

$$\bar{\boldsymbol{u}}_0 = \boldsymbol{N}\,\boldsymbol{v} \tag{57}$$

where matrix $\boldsymbol{N}$ is comprised of the displacement shape functions at the interface between foundation and surrounding soil, and vector $\boldsymbol{v}$ is comprised of the generalized displacements at the nodal rings of the finite element model of foundation. Similarly, the virtual work of the system is obtained by applying the variational principle

$$\delta W = \int_{S_1+S_2} \delta \boldsymbol{t}_0^{\mathrm{T}} \bar{\boldsymbol{u}}_0\,\mathrm{d}\boldsymbol{S} = \delta \boldsymbol{P}^{\mathrm{T}} \int_{S1+S2} \boldsymbol{H}^{\mathrm{T}}\boldsymbol{N}\,\mathrm{d}\boldsymbol{S}\,\boldsymbol{v} = \delta \boldsymbol{P}^{\mathrm{T}}\boldsymbol{B}\,\boldsymbol{v} \tag{58}$$

Equating Eq. (52) to Eq. (58) and factoring out $\delta\boldsymbol{P}^{\mathrm{T}}$, it is obtained.

$$\boldsymbol{Q}\,\boldsymbol{P} = \boldsymbol{B}\,\boldsymbol{v} \tag{59}$$

or

$$\boldsymbol{V} = \boldsymbol{B}\,\boldsymbol{v} \tag{60}$$

where the elements of vector $\boldsymbol{V}$ are the generalized displacements at the nodal rings of the assumed piecewise linear traction model. Eq. (60) gives the relationship between the nodal generalized displacements of the assumed stress model of Eqs. (18) and (20) and the finite element model of Eq. (57). To obtain the corresponding force–stress relationship for both models, the reciprocal theorem can be used. This leads to the following equation:

$$\boldsymbol{F} = \boldsymbol{B}^{\mathrm{T}}\boldsymbol{P} \tag{61}$$

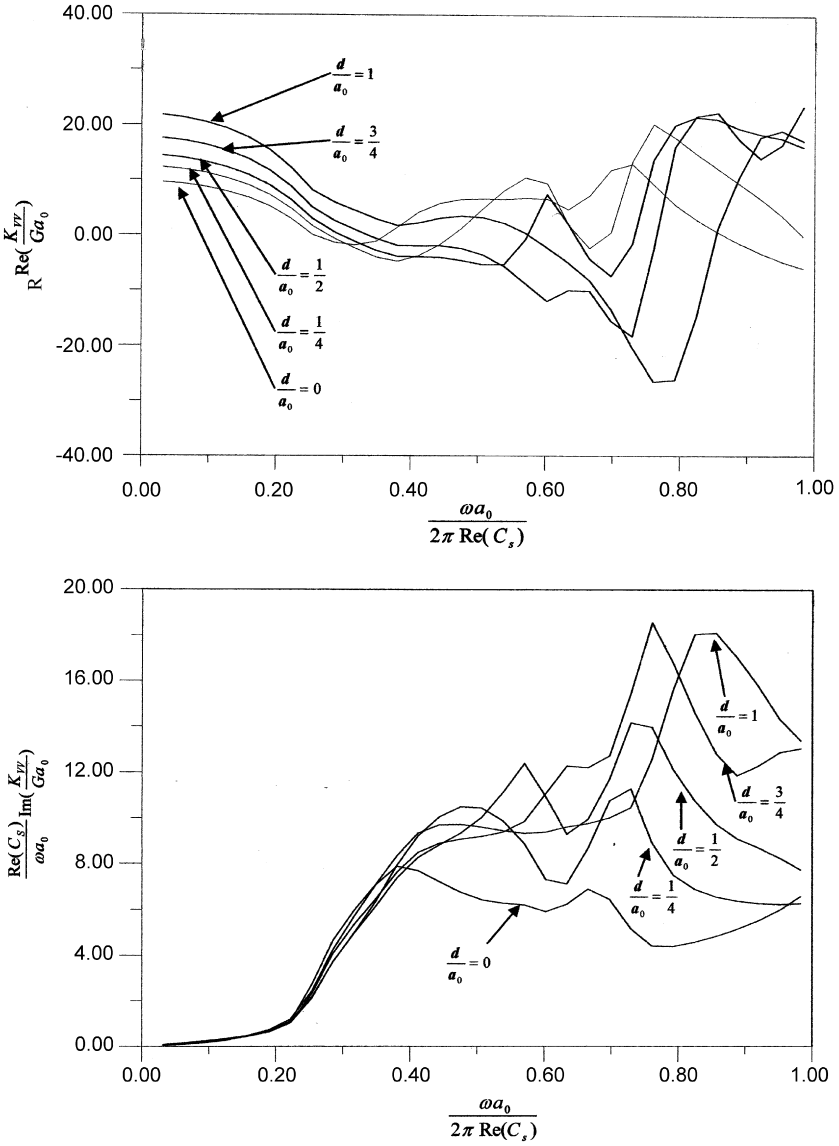

Fig. 9. Non-dimensionalized vertical impedence with different depths for $L/a_0 = 2$.

where the elements of vector $\boldsymbol{F}$ are the generalized forces at the nodal rings of the finite element model. Substituting $\boldsymbol{P} = \boldsymbol{Q}^{-1}\boldsymbol{B}\boldsymbol{v}$ from Eq. (59) into Eq. (61) yields

$$\boldsymbol{F} = \boldsymbol{B}^{\mathrm{T}}\boldsymbol{Q}^{-1}\boldsymbol{B}\,\boldsymbol{v} = \boldsymbol{I}\,\boldsymbol{v} \tag{62}$$

where the matrix $\boldsymbol{I}$ is the impedance matrix for the nth Fourier component. It is noted that $\boldsymbol{I}$ matrix is symmetric matrix.

4. Numerical investigations

A rigid massless circular foundation embedded in a stratum of single layer subjecting to time-harmonic torsional, vertical, rocking and horizontal excitations is used as an example to demonstrate the effectiveness and efficiency of the presented scheme. In this example, 0.05 hysteretic damping ratio is chosen for soil medium and the Poisson ratio of soil is assumed to be 0.33. For the torsional time-harmonic and vertical time-harmonic vibrations of foundation, the anti-symmetric and symmetric Fourier components with $n = 0$ in Eqs. (57), (1) and (2) are involved, respectively in the analysis. For the rocking and horizontal time-harmonic vibrations of foundation, the Fourier component involved in the analysis is the symmetric component with $n = 1$ in Eqs. (57), (1) and (2).

Since the Love modes and Rayleigh modes are involved in the homogeneous solutions, Eqs. (8) and (9) are employed to find the wave numbers for homogeneous solutions of interior domain. And a similar way can be used to find the homogeneous solutions for exterior domain.

To obtain the Love and Rayleigh wave numbers of Eqs. (8) and (9) numerically, Ref. [8] proposed a scheme to locate approximately all the roots in a specified region on complex plane. Then, Mullers [16] method is employed to find the more accurate roots.

For validation of the proposed numerical scheme, the convergence study is performed first. In the study, $L/a_0 = 2$ with $d/d_0 = 0$ (see Fig. 1) and non-dimensional frequency $\omega a_0/(\mathrm{Re}(C_s) = 0.01$ are chosen. The results for the case are shown in Tables 1–5. In these tables, i and j are the numbers of

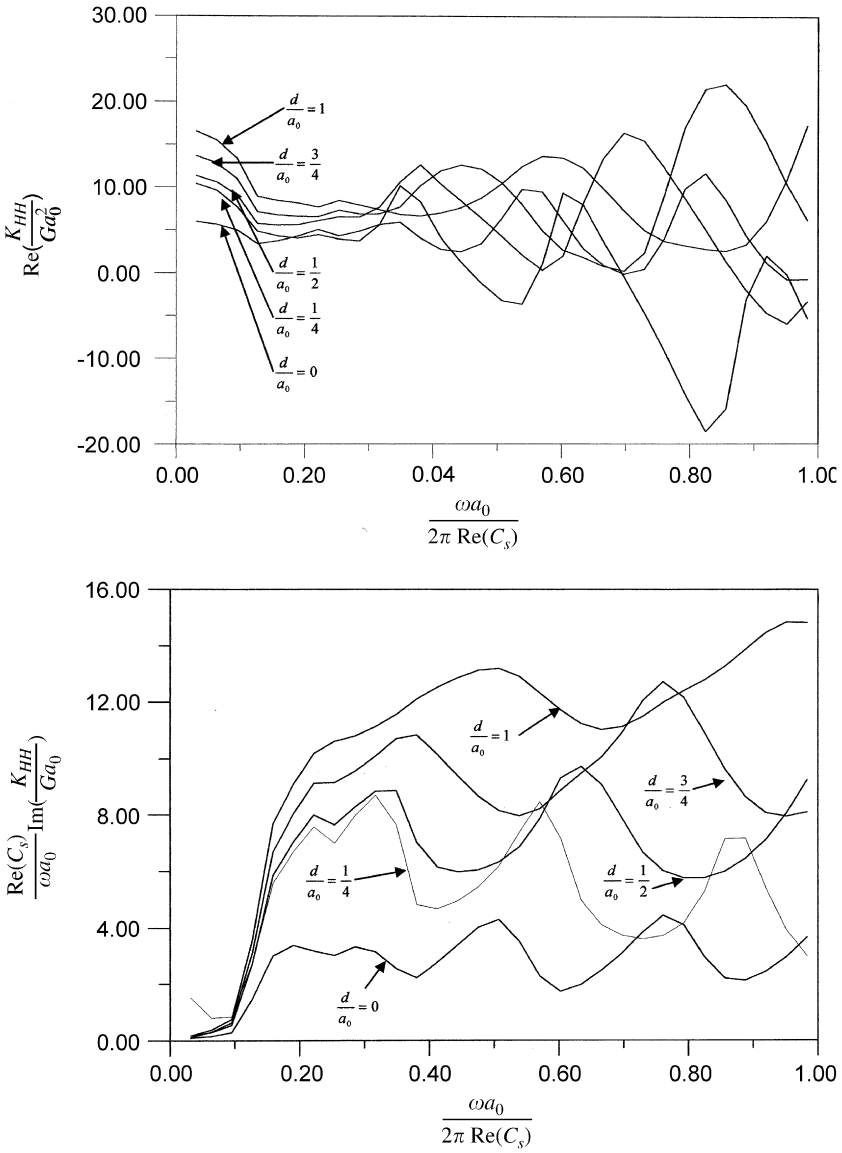

Fig. 10. Non-dimensionalized horizontal impedence with different depths for $L/a_0 = 2$.

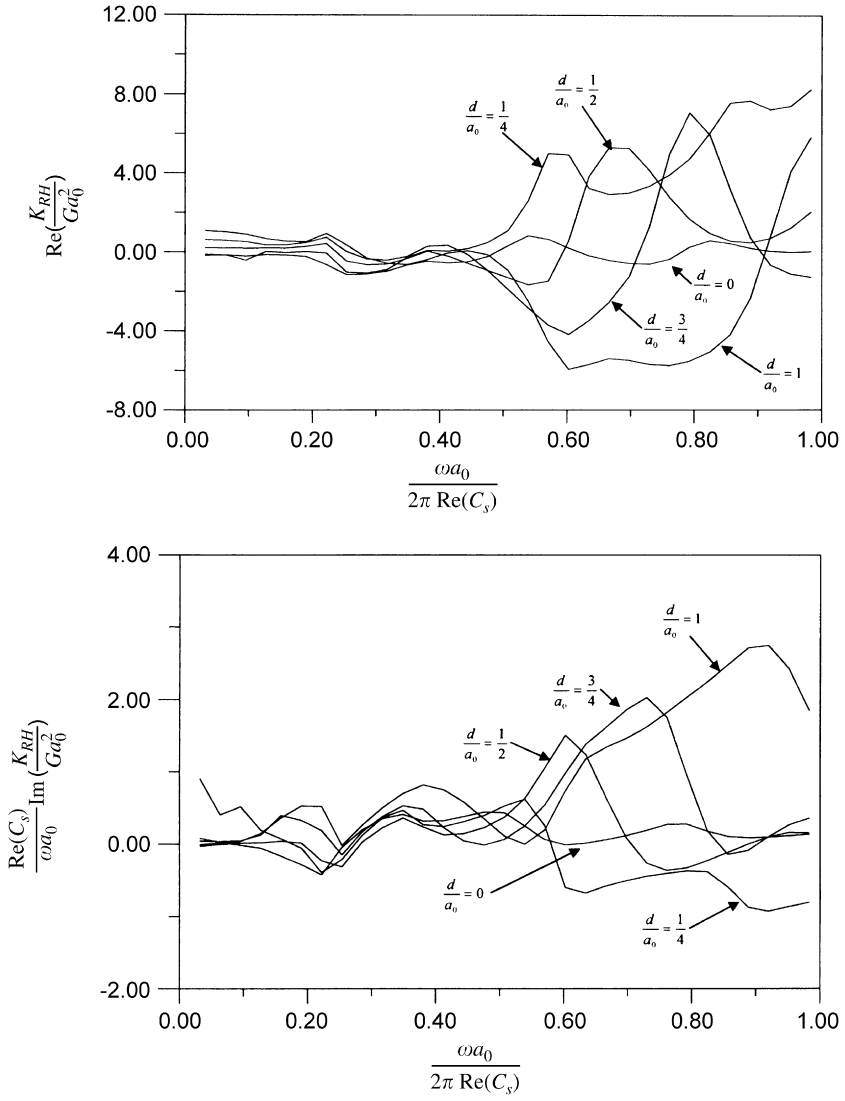

Fig. 11. Non-dimensionalized coupling impedence with different depths for $L/a_0 = 2$.

homogeneous modes for exterior and interior domains, respectively (Eq. (8) or Eq. (9)) used in the analysis, l is the number of particular modes for interior domain (Eq. (22)), m_1 is the number of subintervals for piecewise linear in z direction (Eq. (17)), m_2 is the number of subintervals for piecewise linear in r direction (Eq. (20)), $\mathrm{Re}(C_s)$ is the real part of shear wave velocity of soil medium, K_{TT} is the torsional impedance, K_{VV} is the vertical impedance, K_{HH} is the horizontal impedance, $K_{RH} = K_{HR}$ are the coupling impedance, K_{RR} is the rocking impedance, G is the shear modulus of soil medium and ω is frequency. Also, one should notice that for torsional impedance, i and j are the numbers of Love modes for respective exterior and interior domains, and m_2 and l are the numbers of subintervals and roots of $J_1(ka) = 0$ (Eqs. (22)), respectively for traction $\tau_{\theta z}$, for vertical impedance i and j are the numbers of Rayleigh modes for respective domains, m_2 is the number of subintervals for both tractions τ_{rz} and σ_{zz} and l is the number of roots of $J_0(ka) = 0$ and $J_1(ka) = 0$ (the total number of roots is $2l$), and for horizontal, coupling and rocking impedances, i and j are the numbers of Love or Rayleigh modes for respective domains (the total numbers are $2i$ and $2j$), m_2 is the numbers of subintervals for tractions τ_{rz}, σ_{zz} and $\tau_{\theta z}$ and l is the number of roots of $J_0(ka) = 0$, $J_1(ka) = 0$ and $J_2(ka) = 0$ (the total number of roots is $3l$). In the tables, $i = 10$ and $j = 15$ are enough for exterior and interior domains, respectively, when non-dimensionalized frequency $\omega a_0/(\mathrm{Re}(C_s)) = 0.01$. However, for higher frequency i and j should be larger.

From Tables 1–5, one can see that as l and m_2 become larger, the results are converging and approaching the results of Liou's work [11]. Also one can observe from these tables that the number of particular solutions must be larger than the number of subinterval m_2. This means $l \geqslant m_2+1$. The reason to this restriction is that the number of particular modes employed in the analysis must be greater than the number of unknown nodal intensities of piecewise linear traction. If $l < m_2+1$, then matrix Q in Eq. (52) will be singular.

From the preliminary study, 20 Love or Rayleigh homogeneous modes for both exterior and interior domains are enough for obtaining results of torsional and vertical impedances with good accuracy in the frequency range $\omega a_0/(2\pi\,\mathrm{Re}(C_s)) = 0-1$. For the horizontal, coupling and rocking impedances, 40 homogeneous modes (20 Love modes and 20 Rayleigh modes) are enough for

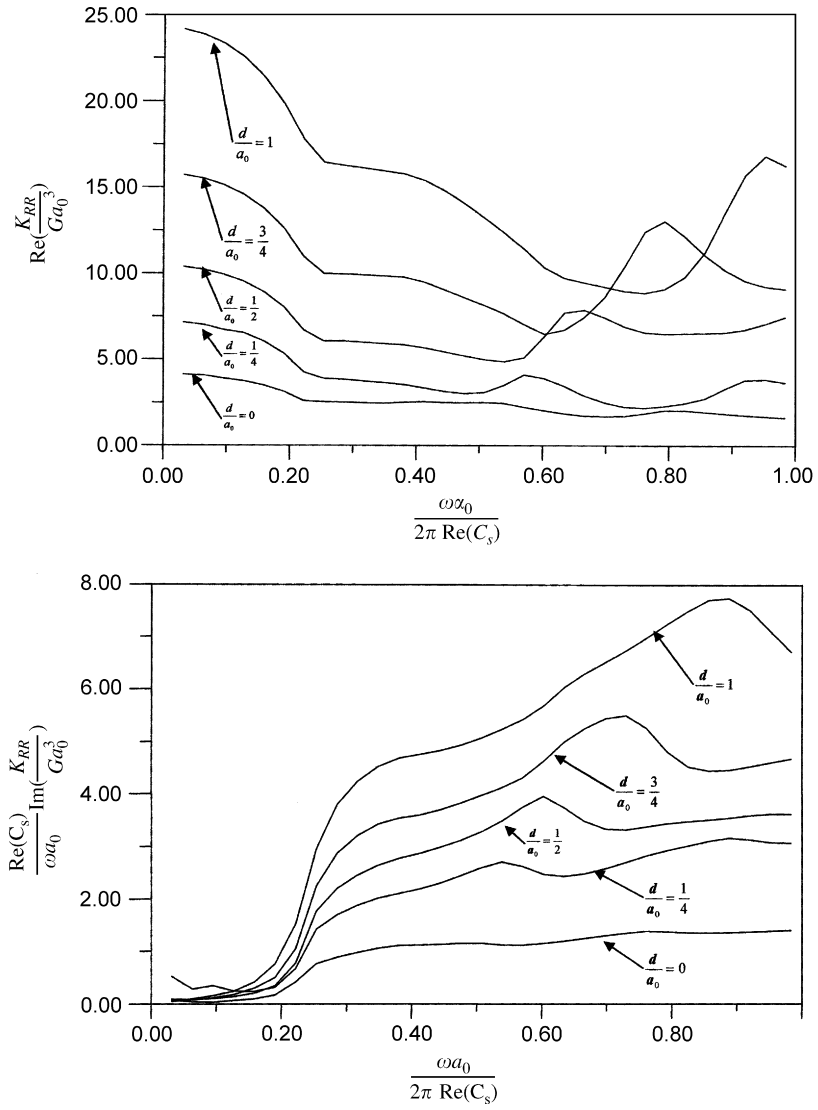

Fig. 12. Non-dimensionalized rocking impedence with different depths for $L/a_0 = 2$.

obtaining results with good accuracy in the frequency range mentioned previously.

For the case of rigid foundation on one layer stratum, Figs. 3–7 show the numerical results of impedance functions with $m_2 = 2$, 3, 4, 5. In these figures, $i = j = 20$ and $l = 6$ are selected after some convergence study has been performed. From these figures, one can observe that the results are approaching the results by Liou and Lee [11], as m_2 becomes larger.

In order to investigate the effects of embedment on impedance functions, the ratios of embedded depth to the radius of foundation (d/a_0) are selected to be 0, $\frac{1}{4}$, $\frac{2}{4}$, $\frac{3}{4}$ and 1. In the investigation, $i = j = 20$, $m_2 = 5$ and $m_1 = 5$, in which m_1 is the number of the subintervals for vertical surface S_1 in Fig. 2, are employed according to the preliminary numerical study . Also, the results for the case $d/a_0 = 1$ are compared to that by Tassoulas and Kausel [14] and good consistency of both results is observed. Figs. 8–12 show the results of torsional, vertical, horizontal, coupling and rocking impedances for rigid circular foundation embedded in one layer stratum. From these figures, one can see that the impedances except coupling impedance are generally getting larger especially in low-frequency range as the embedded depth increases. This means embedment effect is very important.

5. Concluding remarks

After generating torsional, vertical, horizontal, coupling and rocking impedances numerically for foundation embedded in different depth, the following observations can be obtained: (1) The presented scheme can be easily employed to calculate impedances for foundation embedded in a multiple layer stratum. (2) From the above derivation, the scheme can be extended to calculate the impedances for flexible foundation with arbitary shape. (3) The computational cost for generating impedances by the presented scheme is much inexpensive while compared to that by other traditional methods, e.g. finite element method and boundary element method. (4) The presented scheme can also be extended to approximately calculate all impedance functions for foundation in layered half-space medium, if the bottom layer of stratum is thick enough.

Acknowledgment

This work is sponsored by National Science Council of Taiwan under Contract no. NSC 95-2221-E-009-239. The support is greatly appreciated.

Appendix A

The Bessel function matrix $\bar{\boldsymbol{J}}$ in Eq. (5)

$$\bar{\boldsymbol{J}} = \begin{bmatrix} J_n'(kr) & 0 & 0 & 0 & \frac{n}{r}J_n(kr) & 0 \\ 0 & kJ_n(kr) & 0 & 0 & 0 & 0 \\ 0 & 0 & J_n'(kr) & 0 & 0 & \frac{n}{r}J_n(kr) \\ 0 & 0 & 0 & kJ_n(kr) & 0 & 0 \\ \frac{n}{r}J_n(kr) & 0 & 0 & 0 & J_n'(kr) & 0 \\ 0 & 0 & \frac{n}{r}J_n(kr) & 0 & 0 & J_n'(kr) \end{bmatrix} \tag{A.1}$$

in which $J_n(kr)$ is the first kind of Bessel function with order n and $J'(kr) = (\mathrm{d}J_n(kr))/\mathrm{d}r$ The transfer matrices $\boldsymbol{a}_j'$s in Eq. (5) can be expressed as follows:

$$\boldsymbol{a}_j = E_j e(h_j) E_j^{-1} = \begin{bmatrix} \boldsymbol{a}_1 & 0 \\ 0 & \boldsymbol{a}_2 \end{bmatrix} \tag{A.2}$$

in which

$$\boldsymbol{a}_1 = \begin{bmatrix} \frac{2k^2}{k_\beta^2}(CH - CH') + CH & -\frac{k}{k_\beta^2}\left[(2k^2 - k_\beta^2)\frac{SH}{v} - 2v'SH'\right] & \frac{-1}{Gk_\beta^2}\left(v'SH' - k^2\frac{SH}{v}\right) & -\frac{k}{Gk_\beta^2}(CH - CH') \\ \frac{k}{k_\beta^2}\left[2vSH - (2k^2 - k_\beta^2)\frac{SH'}{v'}\right] & CH - \frac{2k^2}{k_\beta^2}(CH - CH') & \frac{k}{Gk_\beta^2}(CH - CH') & -\frac{1}{Gk_\beta^2}\left(vSH - k^2\frac{SH'}{v'}\right) \\ G\left(\frac{4k^2}{k_\beta^2}vSH - \frac{(2k^2 - k_\beta^2)}{k_\beta^2}\left(\frac{SH'}{v'}\right)\right) & \frac{-2kG}{k_\beta^2}(2k^2 - k_\beta^2)(CH - CH') & \frac{2k^2}{k_\beta^2}(CH - CH') + CH' & -\frac{k}{k_\beta^2}\left(2vSH - (2k^2 - k_\beta^2)\frac{SH'}{v'}\right) \\ \frac{2kG}{k_\beta^2}(2k^2 - k_\beta^2)(CH - CH') & G\left(-\frac{(2k^2 - k_\beta^2)^2 SH}{k_\beta^2 \quad v} + \frac{4k^2}{k_\beta^2}v'SH'\right) & \frac{k}{k_\beta^2}\left((2k^2 - k_\beta^2)\frac{SH}{v} - 2v'SH'\right) & CH - \frac{2k^2}{k_\beta^2}(CH - CH') \end{bmatrix} \tag{A.3}$$

and

$$\boldsymbol{a}_2 = \begin{bmatrix} CH' & \frac{SH'}{Gv'} \\ Gv'SH' & CH' \end{bmatrix} \tag{A.4}$$

$CH = \cosh vd_j$, $CH' = \cosh v'd_j$, $SH = \sinh vd_j$, $SH' = \sinh v'd_j$, $K_\beta = \sqrt{\omega^2/C_s^2}$, G is the shear modulus, $v' = \sqrt{k^2 - (\omega^2/C_s^2)}$, $v = \sqrt{k^2 - (\omega^2/C_p^2)}$, C_s is the shear wave velocity and C_p is the compressional wave velocity. Matrices $\boldsymbol{J}_1$ and $\boldsymbol{J}_2$ in Eq. (10) can be expressed as follows:

$$\boldsymbol{J}_1 = \begin{bmatrix} 0 & kJ_n(kr) & 0 \\ J_n'kr) & 0 & \frac{n}{r}J_n(kr) \\ 0 & 0 & 0 \end{bmatrix} \tag{A.5}$$

$$\boldsymbol{J}_2 = \begin{bmatrix} \left(-\frac{J_n'(kr)}{r} + \frac{n^2}{r^2}J_n(kr)\right) & \left(\frac{n}{r}J_n'(kr) - \frac{n}{r^2}J_n(kr)\right) \\ 0 & 0 \\ \left(\frac{n}{r}J_n'(kr) - \frac{n}{r^2}J_n(kr)\right) & \left(-\frac{J_n'(kr)}{r} + \left(\frac{n^2}{r^2} - \frac{k^2}{2}\right)J_n(kr)\right) \end{bmatrix} \tag{A.6}$$

The matrix $\boldsymbol{F}_1 e(z - h_{j-1})E_j^{-1}$ and $\boldsymbol{F}_2 e(z - h_{j-1})E_j^{-1}$ in Eq. (10) can be expressed as follows:

$$\boldsymbol{F}_1 e(z - h_{j-1})E_j^{-1} = \begin{bmatrix} \frac{G}{k_\beta^2}\left(4k^2vSH - (2k^2 - k_\beta^2)^2\frac{SH'}{v'}\right) & -\frac{2kG}{k_\beta^2}(2k^2 - k_\beta^2)(CH - CH') & & \\ \frac{2kG}{k_\beta^2}(-(2v^2 + k_\beta^2)CH + (2k^2 - k_\beta^2)CH') & \frac{G}{k_\beta^2}\left((2k^2 - k_\beta^2)(2v^2 + k_\beta^2)\frac{SH'}{v'} - 4k^2v'SH'\right) & & \\ 0 & 0 & & \\ \frac{2k^2}{k_\beta^2}(CH - CH') + CH' & \frac{k}{k_\beta^2}\left((2k^2 - k_\beta^2)\frac{SH'}{v'} - 2vSH\right) & 0 & 0 \\ \frac{k}{k_\beta^2}\left(2v'SH' - (2v^2 + k_\beta^2)\frac{SH}{v}\right) & \frac{1}{k_\beta^2}((2v^2 + k_\beta^2)CH - 2k^2CH') & 0 & 0 \\ 0 & 0 & Gv'SH' & CH' \end{bmatrix} \tag{A.7}$$

$$\boldsymbol{F}_2 e(z-h_{j-1})E_j^{-1} = \begin{bmatrix} 2G\left(\frac{2k^2}{k_\beta^2}(CH-CH')+CH'\right) & \frac{2kG}{k_\beta^2}\left(2\nu' SH' - (2k^2-k_\beta^2)\frac{SH}{\nu}\right) & 0 & 0 \\ \frac{2}{k_\beta^2}\left(k^2\frac{SH}{\nu}-\nu' SH'\right) & -\frac{2k}{k_\beta^2}(CH-CH') & 0 & 0 \\ 0 & 0 & 2GCH' & 2\frac{SH'}{\nu'} \end{bmatrix} \tag{A.8}$$

References

[1] Tzong TJ, Penzien J. Hybrid modelling of a single-layer half-space system in soil–structure interaction. Earthquake Eng Struct Dyn 1986;14(4):517–30.
[2] Lysmer J, Kuhlemeyer RL. Finite dynamic model for infinite media. J Eng Mech Div 1969;95(4):859–77.
[3] White W, Valliapan S, Lee IK. Unified boundary for finite dynamic model. J Eng Mech Div 1977;95(5):949–64.
[4] Werkel H. Dynamic finite element analysis of three-dimensional soil models with a transmitting element. Earthquake Eng Struct Dyn 1986;14(1):41–60.
[5] Ahmad S, Banerjee PK. Multi-domain BEM for two-dimensional problems in elastodynamics. Int J Numer Methods Eng 1988;26(4):891–911.
[6] Chow YK, Smith IM. Static and periodic infinite solid elements. Int J Numer Methods Eng 1981;17(4):503–26.
[7] Pak RY, Guzina BB. Seismic soil–structure interaction analysis by direct boundary element methods. Int J Solids Struct 1999;36(31):4743–66.
[8] Liou GS. Analytic solutions for soil–structure interaction in layered media. Earthquake Eng Struct Dyn 1989;18(5):667–86.
[9] Liou GS. Vibration of surface foundations of arbitrary shapes. Earthquake Eng Struct Dyn 1991;20(12):1115–25.
[10] Liou GS, Lee GC, Ketter LR. Analytic solution for dynamic loading on half-space. ASCE J Eng Mech 1991;117(7):1485–95.
[11] Liou GS, Lee GC. Impedance matrices for axial symmetric foundations on layered media. Struct Eng Earthquake Eng 1992;9(1):33–44.
[12] Liou GS. Impedance for rigid square foundation on layered medium. Struct Eng Earthquake Eng 1993;10:47–57.
[13] Aviles J, Perez-Rocha LE. A simplified procedure for torsional impedance functions of embedded foundations in a soil layer. Comput Geotech 1996;19(2):97–115.
[14] Tassoulas JL, Kausel E. On the effect of the rigid sidewall on the dynamic stiffness of embedded circular footings. Earthquake Eng Struct Dyn 1983;11(3):403–14.
[15] Wolf JP, Preisig M. Dynamic stiffness of foundation embedded in layered halfspace based on wave propagation in cones. Earthquake Eng Struct Dyn 2003;32(7):1075–98.
[16] de Boor Conte. Elementary numerical analysis; an algorithmic approach. 3rd ed. McGraw-Hill Book Company; 1980.